YALE
PEABODY
MUSEUM

P.O. BOX 208118 | NEW HAVEN CT 06520-8118 USA | PEABODY.YALE. EDU

JOURNAL OF MARINE RESEARCH

The *Journal of Marine Research,* one of the oldest journals in American marine science, published important peer-reviewed original research on a broad array of topics in physical, biological, and chemical oceanography vital to the academic oceanographic community in the long and rich tradition of the Sears Foundation for Marine Research at Yale University.

An archive of all issues from 1937 to 2021 (Volume 1–79) are available through EliScholar, a digital platform for scholarly publishing provided by Yale University Library at https://elischolar.library.yale.edu/.

Requests for permission to clear rights for use of this content should be directed to the authors, their estates, or other representatives. The *Journal of Marine Research* has no contact information beyond the affiliations listed in the published articles. We ask that you provide attribution to the *Journal of Marine Research*.

Yale University provides access to these materials for educational and research purposes only. Copyright or other proprietary rights to content contained in this document may be held by individuals or entities other than, or in addition to, Yale University. You are solely responsible for determining the ownership of the copyright, and for obtaining permission for your intended use. Yale University makes no warranty that your distribution, reproduction, or other use of these materials will not infringe the rights of third parties.

This work is licensed under a Creative Commons Attribution-NonCommercial-ShareAlike 4.0 International License.
https://creativecommons.org/licenses/by-nc-sa/4.0/

Journal of Marine Research, 62, 93–115, 2004

Respiration and vertical carbon flux in the Gulf of Maine water column

by T. T. Packard[1] and J. P. Christensen[2]

ABSTRACT

The transport of carbon from ocean surface waters to the deep sea is a critical factor in calculations of planetary carbon cycling and climate change. This vertical carbon flux can be calculated by integrating the vertical profile of the seawater respiration rate but is rarely done because measuring seawater respiration is so difficult. However, seawater respiratory oxygen consumption is the product of the combined activity of all the respiratory electron transfer systems in a seawater community of bacterioplankton, phytoplankton, and zooplankton. This respiratory electron transfer system (ETS) is the membrane bound enzymatic system that controls oxygen consumption and ATP production in all eukaryots and in almost all bacteria and archaea. As such, it represents potential respiratory oxygen consumption. Exploiting this, we measured plankton-community ETS activity in water column profiles in the Gulf of Maine to give the potential-respiration of the water column. To interpret these potentials in terms of actual seawater respiration we made use of previous measurements of respiratory oxygen consumption and ETS activity in the Gulf of Maine to calculate a ratio of respiratory potential to actual respiration. Armed with this ratio we calculated seawater respiration depth profiles from the ETS activity measurements. These profiles were characterized by: (1) high oxygen consumption rates in the euphotic zone; (2) subsurface maxima near the subsurface chlorophyll maxima (SCM); (3) rapid declines associated with thermoclines; (4) low declining rates below 50 m; (5) and elevated values occasionally near the bottom. Sea surface values ranged from 229 to 489 pmol O_2 min^{-1} L^{-1}. Euphotic zone maximum values ranged from 457 to 682 pmol O_2 min^{-1} L^{-1} while the minimum values below 70 m ranged from 10 to 27 pmol O_2 min^{-1} L^{-1}. A depth-normalized power function described the respiratory profiles between their maxima and minima.

Integrating these respiratory oxygen consumption profiles from the respiratory maximum to the near bottom minimum, we calculated carbon flux profiles. The vertical carbon fluxes through the 30 m, 50 m, and 100 m levels were 3.09 ± 1.55, 1.76 ± 0.96, and 0.93 ± 0.68 μmol C min^{-1} m^{-2}, respectively.

1. Introduction

a. Carbon flux from respiration

Carbon flux at different depths (z) in the ocean can be calculated directly from sediment trap measurements and indirectly from models, by the $^{234}Th/^{238}U$ method, and from the

1. Institut de Ciències del Mar, Pg. Marítim Barceloneta 37-49, 08003 Barcelona, Spain. ***email: ted@icm.csic.es***
2. Bigelow Laboratory for Ocean Science, P.O. Box 475, West Boothbay Harbor, Maine, 04575, U.S.A.

vertical profile of plankton respiration (R). Here we use the latter approach. It dates from Riley's phosphorus model of the North Atlantic (Riley, 1951) and has been used since then by others (Munk, 1966; Packard *et al.,* 1971; Eppley and Peterson, 1979; Jenkins and Goldman, 1985). Jenkin's use of ^{3}He-^{3}H-dating (Jenkins, 1982) to calculate carbon flux from R and the apparent oxygen utilization (Redfield, 1942) brought this approach to the attention of a broad group of marine scientists and renewed interest in assessing respiration in the ocean water column.

The respiration-based method for calculating carbon flux (F_c) achieves its results by integrating the respiration-depth profile ($R = f_R(z)$). $F_c = \int R\, dz = \int f_R(z)\, dz$. It is the reverse of Suess's use of sediment trap profiles (Suess, 1980) to calculate respiration from the first derivative of the carbon flux-depth profile ($F_c = f_c(z)$). $R = dF_c/dz = d(f_c(z))/dz$. In practice, we calculate F_c by integrating R from the bottom of the mixed layer or from some other depth to the sea floor or to infinity. Such calculations of carbon flux do not include benthic R, benthic carbon burial, or the R of large plankton and nekton. Nevertheless, they are consistent with many other calculations and likely represent 90% of the total carbon flux. Here we use enzyme activity measurements of the respiratory electron transfer system (ETS) in the Gulf of Maine (GOM) water column to calculate vertical profiles of R and vertical carbon flux.

b. ETS activity and respiratory oxygen utilization

The use of ETS activity to calculate seawater respiratory processes has recently stirred interest (del Giorgio, 1992; Tortell *et al.,* 1996; Arístegui *et al.,* 2003) because of its high data acquisition rate and because no other technique has the sensitivity to detect community respiratory processes below the euphotic zone. The ETS is not well known outside the field of biochemistry, yet it is one of the most important biochemical processes on the planet. It is composed of pyridine nucleotide dehydrogenases, flavin nucleotide dehydrogenases, and cytochrome-containing oxidoreductases, enzymes that together constitute the fundamental basis of more than 95% of all aerobic and anaerobic respiration. It is a redox process using electron acceptors, such as O_2, NO_3^-, NO_2^-, and SO_4^{-2}, to oxidize the organic products of carbohydrate, lipid, and protein metabolism. Simultaneously it polarizes the biomembrane in which it is housed. The polarized membrane produces the cellular energy-currency molecule, adenosine triphosphate (ATP). The electron acceptors may change according to the environment (e.g., O_2 in ocean surface waters, NO_3^-, NO_2^-, and SO_4^{-2} in oxygen minimum zones and anoxic basins) and the structure and kinetic characteristics of the dehydrogenases and the oxidoreductases may vary with taxonomic phyla. Nevertheless, the fundamental chemistry that catalyzes the oxidation of the nucleotides and reduction of the electron acceptors is the same for phytoplankton, bacteria, and zooplankton. This respiratory ETS (Fruton and Simmonds, 1961; Nelson and Cox, 2000) may be called the electron transport system (Madigan *et al.,* 2000) cytochrome chain, or respiratory chain by different groups of biochemists and microbiologists, but the system is effectively the same. It is organized into four supramolecular lipo-protein

complexes embedded in the inner membrane of mitochondria or the cytoplasmic membrane of bacteria. Each of these complexes catalyzes a different redox reaction along an increasing scale of standard reduction potentials (E°) from E° ($NAD^+|NADH$) = −0.320 V to E° ($O_2|H_2O$) = +0.816 V (Nelson and Cox, 2000) in the case of *R* coupled to oxygen consumption. The electrical work accomplished by the free energy change in these redox reactions is used to drive protons, as H^+, from the inside to the outside of the membrane. With the positively charged protons concentrating on the outside, both a pH and a voltage gradient of about 0.8 pH units and 0.2 V develop across the membrane. These gradients provide enough potential energy to drive a fifth complex (the ATP synthase) to make ATP. During *R,* as two molecules of NADH are oxidized, the complexes transfer 20 protons from the inside to the outside of the membrane. At the same time, the ATP synthase forms 5 to 6 ATP molecules and cytochrome oxidase (complex IV) uses 4 e^- to reduce O_2 to $2H_2O$. It is because of this stoichiometry between the oxygen consumption and the electron flux through the ETS that the ETS is recognized as being the chemical basis of respiratory oxygen consumption (R_{O_2}). When the reaction rate or activity of the ETS is measured, it is done in the presence of a surplus of reactants, the pyridine nucleotides, NADH and NADPH. The result is the respiratory capacity of the ETS, or, in other words, the potential respiration (Φ).

As explained above, the ETS activity is the capacity of a living system to consume oxygen or another electron acceptor. To calculate the actual R_{O_2}, either the enzyme kinetics that control ETS activity or an experimentally determined factor relating respiration to the measured ETS activity, must be applied. This is similar to the problem inherent to any proxy measurement whether it be the $^{18}O/^{16}O$ ratio in foraminifera for paleotemperatures, the thymidine uptake rate in bacteria for bacterial production, or the $^{234}Th/^{238}U$ ratio in ocean particulate matter for carbon flux. All proxies need a reference or calibration. How complicated and difficult this can be is exemplified in the spatial and temporal variability in the algorithms used to convert spectral irradiance, as detected by satellite, into sea-surface chlorophyll concentration, phytoplankton biomass, and phytoplankton productivity. The use of ETS activity as a proxy for ocean R_{O_2} and as a way to calculate vertical carbon flux has not been explored as extensively as has been chlorophyll for phytoplankton biomass or the $^{234}Th/^{238}U$ ratio for the determination of carbon flux. This investigation is a part of this exploration process and an attempt to address this imbalance.

Calculating R_{O_2} from potential respiration (Φ) requires the application of either bisubstrate enzyme kinetics (Packard *et al.,* 1996) or an empirically determined ratio of R_{O_2} to Φ. Since Φ is related to ETS activity by a stoichiometrically determined constant, one can use, as well, a coefficient ($C_{R/ETS} = R_{O_2}/ETS$) that relates R_{O_2} to the ETS activity. On this expedition to the GOM, it was not feasible to use the kinetic approach (Packard *et al.,* 1996) nor to repeat the experiment we made in 1980 (Packard and Williams, 1981); the personnel and the resources were simply not available. However, since we were working in the same relative location, we assumed that we could use the results from our previous experiment (Packard and Williams, 1981) to calculate $C_{R/ETS}$. We assumed for heuristic

Table 1. Station summary of the location and seawater characteristics for the R/V *Endeavor* cruise EN376, September 2002. See Hopkins and Garfield (1979) for a chart of the GOM and neighboring waters.

CTD station number	Position	Depth (m)	*T* sea surface (°C)	*T* 25 m (°C)	1% light level (m)	Surface salinity (PSU)	Surface chlorophyll (mg L^{-1})	Surface respiration (pmol O_2 $min^{-1}L^{-1}$)	Depth of chlorophyll maximum (m)
10	42° 35.7′N 69° 31.1′W	266	16.44	8.66	42	32.39	0.99	229	15
12	42° 35.2′N 69° 31.8′W	275	16.66	13.06	*	32.41	1.46	396	20
14	42° 34.8′N 69° 31.4′W	273	16.33	12.95	*	32.41	1.45	481	25
42	42° 57.4′N 65° 49.9′W	147	14.12	12.99	19	33.12	4.66	437	10
48	42° 57.6′N 65° 50.5′W	155	12.06	11.51	*	32.95	12.3	489	0

*Night station.

purposes that the temporal variability around $C_{R/ETS}$ is minimal. Then, applying this coefficient to five vertical ETS activity profiles, we calculated the corresponding respiration profiles. Next, we calculated carbon flux by integrating the R_{O_2} profiles. This was done several ways to facilitate comparison with the literature. Our approach differs from others in that it yields results on a time scale of minutes. Furthermore, by generating detailed R_{O_2} profiles, integrations can be carried out to any depth within the range of the measurements enabling carbon flux profiles to be constructed over the entire range of the profiles.

2. Methods

a. Sampling

Two GOM time-series stations were occupied. Three casts for ETS activity were taken in Wilkinson Basin (42° 35.6′N, 69° 31.5′ W) in 275 m of water for the first time series and two were taken on the Scotia shelf south of Cape Sable, Nova Scotia (42° 57.5′N, 65° 50.3′W) in 155 m of water for the second time series. The samples for ETS activity were taken with 10-L Niskin bottles mounted on a Sea-Bird rosette (SBE-9 plus). Other measurements were made simultaneously by the R/V *Endeavor's* SEASOFT data acquisition system. A Sea Tech flash lamp fluorometer measured chlorophyll, a WET labs C-Star transmissometer (25 cm pathlength) measured seawater optical transmission, a Biospherical Instruments radiometer (QSP-200L4S) measured subsurface solar radiation, and a SBE-13 O_2 electrode measured seawater O_2. Station positions are given in Table 1. Transmissometer readings (T_m) on a scale of 0 to 100 were converted into an index of seawater turbidity (T_r) by the expression, $T_r = (100\text{-}T_m)$.

b. ETS activity

Ten to twelve ETS samples from each cast were drawn into 2 L acid-rinsed polycarbonate bottles without prefiltration. This practice was consistent with our previous sampling protocol (Packard and Williams, 1981) and facilitated use of prior results to interpret our ETS measurements. After processing the samples from each cast, the empty sampling bottles were rinsed with 5% HCL and stored at 7°C, in the dark until the next cast. Then the bottles were rinsed three times with *in situ* seawater before sampling again. Sample filtration began within an hour after the cast and took 2 h to process the 12 two-L samples and 3 one-ml filter blanks. It was done at a pressure differential of $<1/3$ atm at laboratory temperature (21°C) using Whatman GF/F 42.5 mm glass fiber filters with a nominal pore size of 0.7 μm. After filtration, the filtration apparatus was rinsed with filtered seawater and the presence of zooplankton noted. The filter was folded to an eighth, blotted thrice to remove excess seawater, placed in a capped cryovial, and stored for a few days in liquid N_2 until measurement. Homogenates were prepared as before (Packard and Williams, 1981) and analyzed within 5 min. As in our earlier work in the GOM we never stored homogenates or ran assays in a batch mode.

Seawater for ETS filter-blanks was drawn in triplicate from the filtrate of the deepest sample. For each filter-blank 1 ml of this filtered seawater was refiltered through a new GF/F 42.5 mm glass fiber filter. The filter was then treated and stored as described. The mean of these three filter-blanks served as the control for the analysis of each station's ETS analyses. For the five stations the mean and standard deviation was 0.0012 ± 0.0002 absorbance units per min per filter. This value served as the level of sensitivity for the ETS analyses here. Except for one, all the samples exceeded this limit by a factor of 2.

ETS activity was measured as before (Packard and Williams, 1981) with the following modifications to save time and resources. Reagent and reaction volumes were a fifth of the original volumes. Succinate, shown not to be an important reactant in seawater analysis (Savenkoff *et al.,* 1995), was eliminated. Absorbance was detected at 520 nm rather than 490 nm, but since the INT-formazan absorbance peak on the spectrophotometer is so broad, the difference is negligible (1%). The assay was done kinetically, one depth at-a-time to avoid any enzymatic degradation of the homogenate. The most linear portion between 4 and 12 min was usually chosen for the slope calculation. The coefficients of determination (r^2) were nearly always greater than 0.998. A composite of the absorbance measurements from station 48 is shown in Figure 1. R_{O_2} and Φ at the incubation temperature (21.5°C) are directly proportional to these slopes.

Calculations of ETS activity (nmol e^- min^{-1} L^{-1}) and Φ (nmol O_2 min^{-1} L^{-1}) from the initial absorbances were done as previously described (Packard and Williams, 1981). The measurement exploits the preferential reduction of the tetrazolium dye, INT (2-p-iodophenyl-3-p-nitrophenyl-5-phenyl monotetrazolium chloride), by the respiratory ETS. The rate of electron transfer is followed stoichiometrically by the absorbance between 490 and 520 nm as the yellow tetrazolium is reduced to a formazan, the dye's red form. The tetrazolium, accepting two electrons, replaces O_2 as the electron acceptor for the ETS. Oxygen would

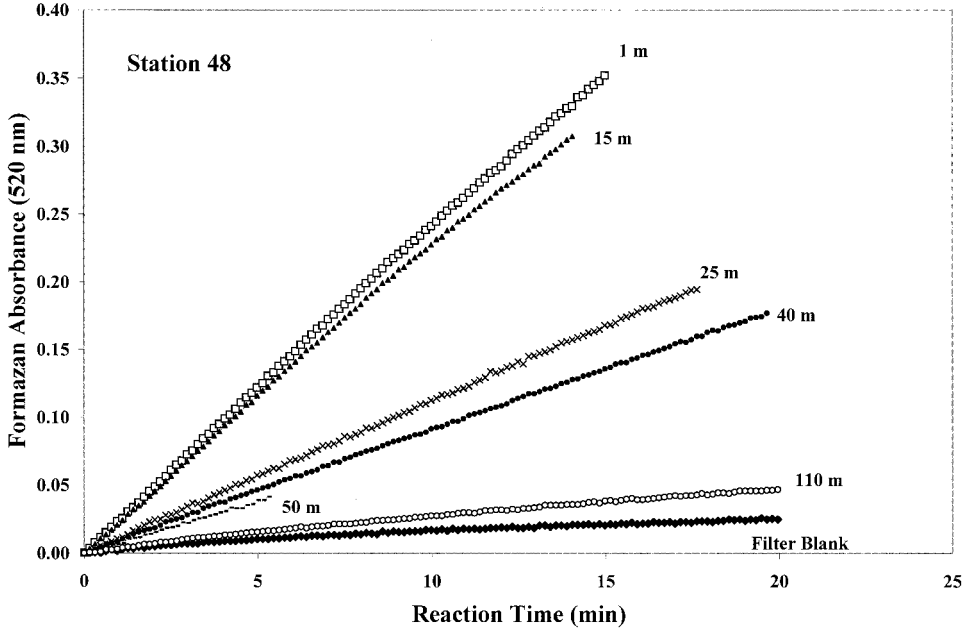

Figure 1. ETS activity for six different depths at station 48 on the Scotia Shelf. The Y-axis represents formazan optical density in a 1 ml cuvette with a 1 cm path length. The slope is directly proportional to ETS activity, Φ, and R_{O_2}. These time-courses serve as demonstrations of the linearity of INT reduction and formazan production over 15 min. To avoid slowing the reaction by reactant limitation, measurements are stopped before the formazan absorbance exceeds 0.450. Instrument failure limited the 50 m ETS reaction.

normally accept 4 electrons in the absence of INT. However, when offered INT, the ETS reduces it instead of O_2. Thus, on a molar basis, the formazan production rate (nmol formazan $min^{-1} L^{-1}$) is equivalent to twice the rate of Φ (nmol O_2 $min^{-1} L^{-1}$) and 1/2 the ETS activity (nmol e^{-1} $min^{-1} L^{-1}$). Φ and R_{O_2} were corrected for changes in the water column temperature, *T,* by an application of the Arrhenius equation (Packard *et al.,* 1975; Arístegui and Harrison, 2002). Table 2 summarizes the calculation of ETS activity, Φ, R_{O_2}, as well as the temperature correction from the primary formazan-absorbance measurements. The precision of duplicate measures of ETS (Table 3) was $\pm 7.8\%$ of the mean. R_{O_2} (pmol O_2 $h^{-1} L^{-1}$) for all five stations is given in Table 3; it was calculated from the relationship between Φ and seawater R_{O_2} for the euphotic zone of the GOM (Fig. 2). We (Packard and Williams, 1981) originally reported a unitless ratio of R_{O_2} to ETS activity of 0.343 ± 0.041 ($n = 21$). However, when the seven fractionated samples are excluded so that only the whole plankton samples ($n = 14$) are considered, this ratio ($C_{R/ETS}$) becomes 0.287 (Fig. 2). When these data are replotted to pass through zero, $C_{R/ETS}$ (unitless) becomes 0.260 (Fig. 2). This ratio was used as in Table 2 to convert Φ to R_{O_2} (Table 3).

Table 2. Calculations of ETS activity and water column respiration (R_{O_2}) from primary time-dependent tetrazolium-reduction measurements from station 10. Depth is z and seawater volume filtered is V. Third column lists rates of formazan production (tetrazolium reduction) as increases in absorbance at 520 nm. Values are corrected for filter-blank (FB) absorbance. The formazan production rate in nmol min^{-1} L^{-1} (4^{th} column) is the third column divided by the specific absorbtivity of INT-formazan, 15.9 (Kenner and Ahmed, 1975). ETS activity in nmol e^{-1} min^{-1} L^{-1} (column 5) is the formazan production rate multiplied by 2. Potential-respiration (Φ) in nmol O_2 min^{-1} L^{-1} (column 6) is the formazan production rate divided by 2. Column 6 lists Φ at reaction T (21.5°C). Column 7 lists Φ at *in situ T*. The latter calculation employs the Arrhenius equation (Packard *et al.,* 1971; 1975). R_{O_2} at 21.5°C and *in situ T* are listed in columns 8 and 9. They were calculated from Φ in columns 6 and 7 using the slope ($C_{R/ETS}$) from line 2 in Figure 2 (0.26).

		Formazan Production Rate		ETS Activity	(Φ) nmol O_2 min^{-1} L^{-1}		(R_{O_2}) nmol O_2 min^{-1} L^{-1}	
z (m)	V (L)	(ΔA_{520}-FB) (V $min)^{-1}$	nmol min^{-1} L^{-1}	nmol e^- min^{-1} L^{-1}	at 21.5°C	at *in situ* temp	at 21.5°C	at *in situ* temp
5	2.0	0.00428	2.83	5.66	1.41	0.882	0.368	0.2293
5	2.0	0.00383	2.53	5.06	1.27	0.789	0.329	0.2052
10	2.0	0.00528	3.49	6.98	1.74	1.051	0.453	0.2733
10	2.0	0.00418	2.76	5.53	1.38	0.833	0.359	0.2164
15	2.0	0.00978	6.46	12.92	3.23	1.758	0.840	0.4569
25	2.0	0.00133	0.88	1.76	0.44	0.129	0.114	0.0334
30	2.0	0.00118	0.78	1.56	0.39	0.111	0.102	0.0288
35	2.0	0.00073	0.48	0.97	0.24	0.067	0.063	0.0175
40	2.0	0.00073	0.48	0.97	0.24	0.062	0.063	0.0161
70	2.0	0.00053	0.35	0.70	0.18	0.040	0.046	0.0105
75	3.8	0.00049	0.32	0.65	0.16	0.038	0.042	0.0100

3. Results

a. Sea water characteristics

Wilkinson Basin surface seawater was warm (16.50 ± 0.16°C), low in chlorophyll (1.0–1.5 ug/L), and moderate in R_{O_2} (205–481 pmol O_2 min^{-1} L^{-1}). The water column was stratified with a 6° T decrease in the thermocline between 15 and 25 m at station 10 and between 15 and 40 m at stations 12 and 14. A 4.4°C T rise at 25 m in 8 h at the same location (stations 10 and 12) suggests internal waves added variability to the profiles at this time-series station. However, all three stations here featured a subsurface chlorophyll maximum (SCM) of 4.0 ± 0.5 ug/L at the top of the thermocline (Table 1) consistent with the observation of (Prahl *et al.,* 2001).

Scotia Shelf surface seawater was colder (13.0 ± 1.0°C) and higher in both chlorophyll (7–12 ug/L) and R_{O_2} (437–489 pmol O_2 min^{-1} L^{-1}). The salinity at the sea surface was slightly higher on the Scotia shelf (33.00 psu) than over the Wilkinson Basin (32.40 psu). The water column was weakly stratified with only a 1–2°C T decrease in the upper 50 m and a chlorophyll maximum in the upper 15 m (Fig. 4). At station 48 the chlorophyll

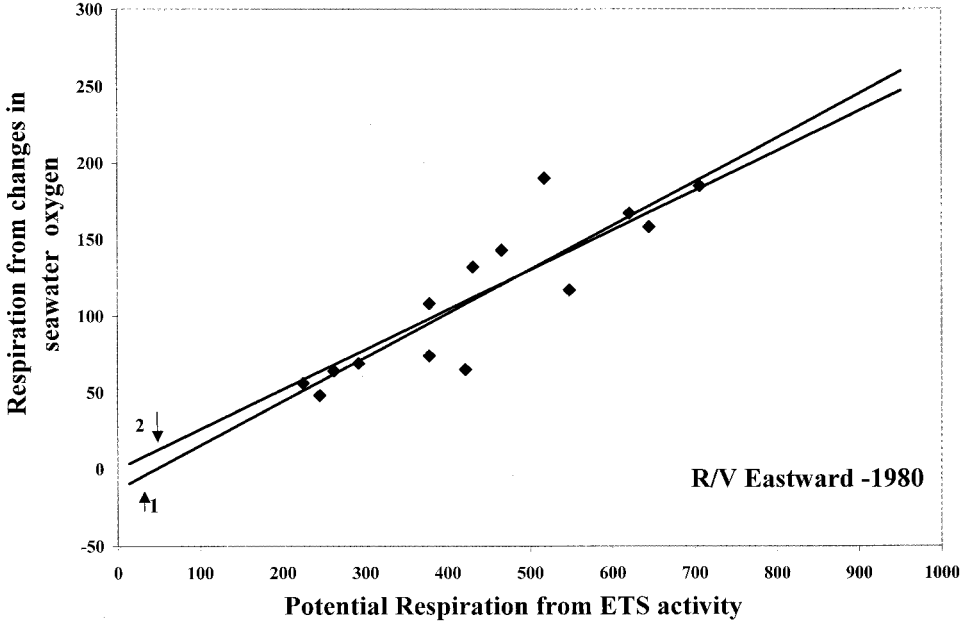

Figure 2. R_{O_2} versus Φ for the GOM, July 1980. Data were the 14 paired measurements of Φ, based on seawater ETS activity, and R_{O_2}, directly measured from O_2 utilization in bottled seawater samples (Table 2 of our previous study (Packard and Williams, 1981)). The units are $\mu g\ O_2\ L^{-1}\ d^{-1}$, but the slope is unitless. Regression line #1 is: $R_{O_2} = 0.287\ \Phi - 13.258$ ($r^2 = 0.774$). However, the slope is not significantly different from zero, so when we take the intercept as zero, we calculate line #2 which is: $R_{O_2} = 0.260\ \Phi$ ($r^2 = 0.766$). This slope, $R_{O_2}/\Phi = 0.260$, was used to calculate R_{O_2} in this paper.

maximum was at the surface. At 100 m the *T* here, at 11.5°C, was 5°C warmer than at Wilkinson Basin. At both the shelf and the basin stations, e.g., as at station 14 (Fig. 3), the water-column density and salinity profiles displayed a gradual increase with depth that was completely unlike the R_{O_2} profile.

b. ETS activity, potential-respiration, and respiration

The ETS activity measurements as both nmol formazan produced $min^{-1}\ L^{-1}$ and nmol $e^{-1} min^{-1}\ L^{-1}$ as well as Φ and R_{O_2} as nmol $O_2\ min^{-1}\ L^{-1}$ for station 10 are given in Table 2. R_{O_2} in pmol $O_2\ min^{-1}\ L^{-1}$ for all stations is given in the Table 3. Table 2 serves as a step-by-step example of how ETS activities, measured as absorbance changes per minute, convert to seawater R_{O_2} in nmol $O_2\ min^{-1}\ L^{-1}$. ETS activity, Φ and R_{O_2} are related by constants so that a relationship found for ETS activity also holds for R_{O_2} or Φ. Also, the preferred units for ETS activity are in nmol e^- rather than in nmol O_2; we reserve O_2-based units for Φ and R_{O_2}. This practice was not followed in the past and led to confusion. Standard biochemical shorthand for enzyme activity, "unit," (μ mol of product produced

Table 3. R_{O_2} profiles in the GOM water column, September 2002. R_{O_2} has been corrected for *in situ T* as in Table 2; here R_{O_2} is reported as pmol O_2 min^{-1} L^{-1}. Depth is z.

Station 10		Station 12		Station 14		Station 42		Station 48	
z (m)	R_{O_2}	z (m)	R_{O_2}	z (m)	R_{O_2}	z (m)	R_{O_2}	z (m)	R_{O_2}
5	229	1	396	2	481	1	437	1	489
5	205	10	502	3	426	5	449	15	438
10	273	15	436	10	409	10	642	25	200
10	216	25	223	20	416	10	682	40	156
15	457	30	302	25	364	15	520	44	155
25	33	30	242	30	225	20	296	50	136
30	29	40	37	40	74	30	128	75	30
35	18	50	13	50	14	40	70	90	38
40	16	100	14	100	16	50	51	110	27
70	11	250	12	200	12	60	61	145	27
75	10	265	29	230	12	80	13		
						130	56		
Bottom z 266 m		Bottom z 275 m		Bottom z 273 m		Bottom z 147 m		Bottom z 155 m	

per min), is avoided because "unit" by itself is meaningless to most marine scientists. In contrast, units that specifically identify the reactants consumed (i.e., O_2) or product formed (i.e., CO_2), over a stated time period (i.e., min), and normalized by seawater volume or sea surface area, are not only more explicit, but more readily understood.

R_{O_2} often increases from the surface to some subsurface maximum near the SCM (Table 3 and Fig. 4). From this maximum, R_{O_2} decreases by a factor of 20–50 through the thermocline and more gradually below it. Near the bottom it increases at some stations (Table 3). The decrease through the thermocline and into the deeper waters can be described by power functions ($R_z = R_0 z^b$), by depth-normalized power functions ($R_z = R_t(z/z_t)^b$) and by exponential functions ($R_z = R_0 e^{bz}$). In each function, R_z is the R_{O_2} (nmol O_2 min^{-1} L^{-1}) at any depth (z) and b is the curvature of the profile; b is always negative. The constants, R_0, R_t, and z_t represent the modeled sea surface R_{O_2}, the modeled R_{O_2} at the top of the depth interval to be considered, and the top depth of the same interval, respectively. Table 4 presents equations for the exponential and the power function that best fit R_{O_2} data from the subsurface R_{O_2} maximum to the deepest measurement. Note that the modeled values are higher than the measured values at the surface, but are equal at z_t (Table 3). The equations should only be used below the R_{O_2} maximum ($z = z_t$). Note also that at depth the modeled R_{O_2} by the exponential function tends to be low (Fig. 5). That is one reason why the depth-normalized power function ($R_z = R_t(z/z_t)^b$) is used later to calculate carbon fluxes. Martin argued that one advantage of this depth-normalized function is that R_{O_2} at $z = z_t$ is close to the measured value at z_t (Martin *et al.,* 1987). This is true, however, as Figure 5 shows, it does not fit the data any better than the simple power function; both b and r^2 are equal. Figure 5 gives examples of both power functions and

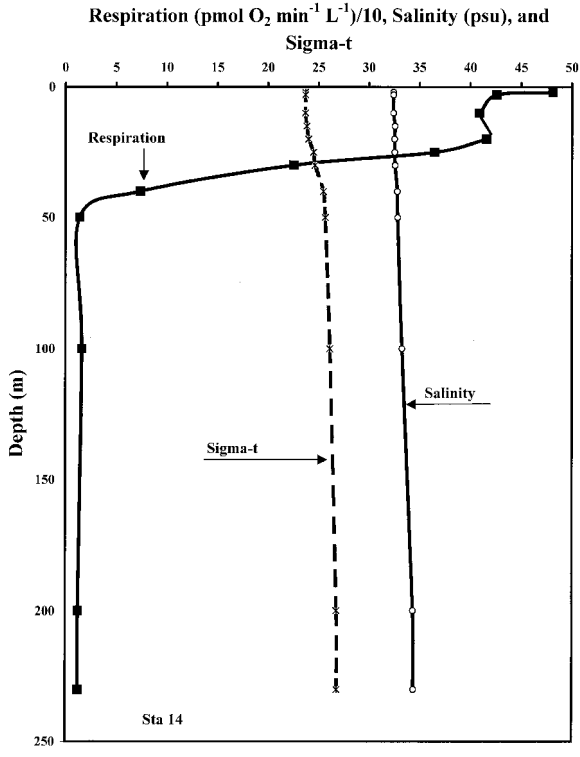

Figure 3. Profiles of density (sigma-*t*), salinity (psu), and R_{O_2} (pmol O_2 L^{-1} min^{-1})/10 at station 4.

exponential functions at station 48 where they both describe R_{O_2} relatively well (r^2 = 0.9535 and 0.8778) and where at station 12, they describe it relatively poorly (r^2 = 0.8403 and 0.5933). However, in both examples the power functions fit the data at the top and the bottom of the profiles better than do the exponential functions.

c. Chlorophyll, turbidity, and respiration

ETS activity in plankton is known to be related to living biomass as well as to chlorophyll (Packard *et al.,* 1974, 1983, 2000). Thus, when seawater chlorophyll is high, ETS activity and R_{O_2} in the water column should also be high. In general, this was the case at our stations on the Scotia shelf, but because of the high R_{O_2} above the chlorophyll maxima, it was not the case in Wilkinson Basin (Table 5). Chlorophyll and R_{O_2} correlate well at stations 42 and 48 (Scotia Shelf), but not at stations 12 and 14 (Wilkinson Basin). Examples of good (station 42) and bad (station 12) correlation can be seen by inspecting the profiles in Figure 4.

Turbidity (T_r), a rough index of suspended and dissolved material in seawater, would be correlated with seawater ETS activity and R_{O_2} if a large fraction of this material is living. If

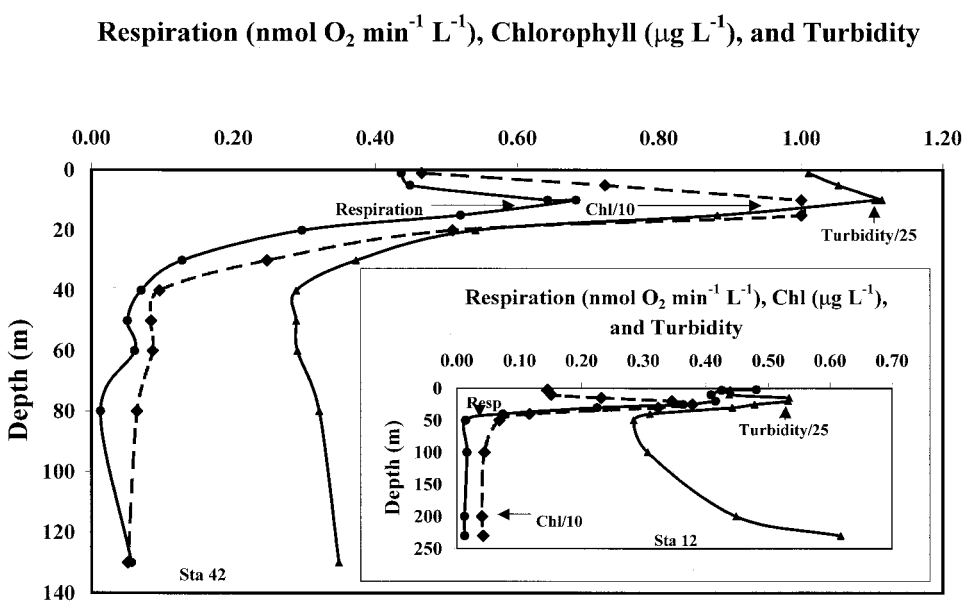

Figure 4. Profiles of T_r/25, chlorophyll (μg L^{-1})/10, and respiration (nmol O_2 L^{-1} min^{-1}) at station 42 (Scotia Shelf) and 12 (Wilkinson Basin) as examples of the covariation of these three variables in the upper water column.

the material were dead, there would be no correlation. On the Scotia shelf (Fig. 4 and Tables 6 and 7) T_r is well correlated with both chlorophyll and R_{O_2} indicating that the suspended material is largely living phytoplankton or covaries with it. In Wilkinson Basin, T_r is better correlated with R_{O_2} than with chlorophyll indicating the greater presence of bacteria and zooplankton in the suspended material. R_{O_2} at stations 12 and 14 has twin maxima, unlike chlorophyll; this is additional evidence for nonalgal living biomass. At all stations we observed many small copepods on the GF/F filters, so part of the respiratory signal at all stations is due to them. Had we pre-filtered the samples, the chlorophyll-R_{O_2} relationship might have been closer, but then our methodology would have departed from our previous GOM study (Packard and Williams, 1981). It should be noted that a good correlation between ETS-based R_{O_2} and chlorophyll in a seawater sample does not preclude the importance of the ETS-based R_{O_2} in bacteria and zooplankton. It simply means that the phytoplankton R_{O_2} dominates in the plankton community or that the R_{O_2} of the other members of the community covaries with the phytoplankton R_{O_2}.

Co-occurrence of ETS activity maxima and transmissometer minima were observed in our early work in the deep waters of the eastern tropical Pacific (Garfield *et al.,* 1983). The transmissometer minima were T_r maxima and are an index of particle maxima. The increased ETS activity indicated microbe maxima. Here, in these relatively shallow coastal waters of the GOM, T_r maxima are also related to ETS activity and R_{O_2} (Table 6). In addition, they are related to chlorophyll (Table 7 and Fig. 4). Note that at all stations, the r^2

Table 4. Exponential ($R_{O_2} = R_0 e^{bz}$) and power function ($R_{O_2} = R_0 z^b$) best fits to the R_{O_2} depth profiles from cruise EN376. Depth (m) is z; Δz is the depth range over which each equation is valid; and n is the number of R_{O_2} measurements used. Only R_{O_2} values that decreased continuously from the respiration subsurface maximum to the bottom measurement were considered (Table 3). The coefficient, R_0, represents the predicted surface R_{O_2} for $z = 0$ or 1 for the exponential and power function, respectively. The exponent (b) controls the curvature. Large negative values of b force R_{O_2} to decrease rapidly from euphotic zone values, low values of b force R_{O_2} to decrease slowly from euphotic zone values.

Exponential $R_{O_2} = R_0 e^{bz}$	Station	R_0 (nmol O_2 min^{-1} L^{-1})	b	r^2	n	Δz
	10	0.17	−0.044	0.577	7	15–75
	12	0.18	−0.011	0.421	10	10–265
	14	0.19	−0.014	0.566	8	20–230
	42	0.35	−0.024	0.519	9	10–130
	48	0.37	−0.022	0.878	9	15–145
Power $R_{O_2} = R_0 z^b$	Station	R_0 (nmol O_2 min^{-1} L^{-1})	b	r^2	n	Δz
	10	45.93	−2.063	0.789	7	15–75
	12	6.96	−1.172	0.683	10	10–265
	14	23.47	−1.487	0.775	8	20–230
	42	15.33	−1.378	0.791	9	10–130
	48	20.65	−1.382	0.954	9	15–145

values in Table 6 reveal a stronger T_r-R_{O_2} relationship than either the chlorophyll-R_{O_2} or the chlorophyll-T_r relationships. Again, this could be expected because both the transmissometer and the ETS assay will detect not only phytoplankton cells, but also bacteria, protozoa, and zooplankton. As with the chlorophyll (Chl) profiles, Figure 4 shows good (station 42) and poor (station 12) examples of correlation in vertical profiles between T_r and R_{O_2}.

d. Carbon flux

For the calculation of the respiratory CO_2 production rate (R_{CO_2}) from R_{O_2}, we have previously used the C/O ratio of 0.69 (Takahashi *et al.,* 1985) rather than the classic Redfield C/O ratio of 0.77 (Packard *et al.,* 1988, Christensen *et al.,* 1989). Here, we use the same ratio to calculate the R_{CO_2} (μmol C min^{-1} m^{-3}) and from these data we generate the equations for the depth-normalized power function $R_z = R_t(z/z_t)^b$ (Table 8). In these equations, R_t is R_{CO_2} in μmol C min^{-1} m^{-3} at the upper depth (z_t) to which the equations apply. The bottom of the euphotic zone occurs at about 30 m. Since most of the seasonal thermocline as well as the maxima for chlorophyll, T_r, and R_{O_2} are found above this depth, we chose it as a starting point for carbon export to depth. The R_{O_2}, Chl, and the T_r maxima above it argue for relative stability in the euphotic zone during the days preceding the sampling. In addition to this 30 m level, we calculated the carbon export from the 50 and 100 m levels to facilitate comparison with fluxes based on sediment traps, ^3H-^3He dating,

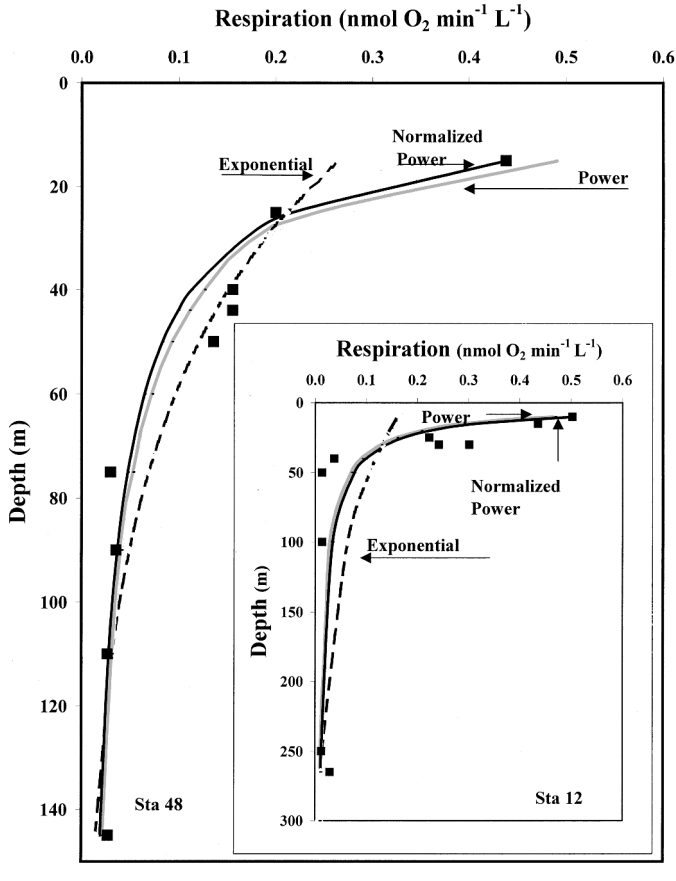

Figure 5. R_{O_2} depth profile from 15 to 145 m at station 48. The power function ($R_{O_2} = 20.65\, z^{-1.3815}$, $r^2 = 0.954$) fits the profile better than the exponential function ($R_{O_2} = 0.37\, e^{-0.0224z}$, $r^2 = 0.878$) both at depth and in the upper 30 m. The power function normalized by the depth of the R_{O_2} maximum ($R_{O_2} = 0.438\,(z/15)^{-1.3815}$), fits the data (■) as well as the simple power function and the r^2 at 0.954 is equal. **Inset:** R_{O_2} depth profile from the R_{O_2} maxima (10 m) to the bottom depth (275 m) at station 12. As with station 48, neither the power function ($R_{O_2} = 6.96\, z^{-1.1716}$, $r^2 = 0.840$) nor the exponential function ($R_{O_2} = 0.18\, e^{-0.0105z}$, $r^2 = 0.593$) fit the profile well between 50 and 100 m, but the power function is clearly better above 40 m. The power function normalized by the depth of the R_{O_2} maximum ($R_{O_2} = 0.502\,(z/10)^{-1.1716}$), fits the data (■) as well as the simple power function and their r^2 values at 0.840 are equal. **Both plots:** Note that R_{O_2} is expressed as nmol O_2 L^{-1} min^{-1}. As with the other stations, the data between the surface and the R_{O_2} maximum was not considered in the analysis.

and mass balance models (Table 9). Our carbon flux calculations were made in three ways to facilitate comparison with other determinations and to heuristically demonstrate the variability in the different integrations. First, we integrated R_{CO_2} from 30, 50, and 100 m to the bottom by trapezoidal approximation. Reported as F_{trap}, these carbon fluxes, in μmol C

Table 5. R_{O_2} (Table 3) as a function of chlorophyll in the form, $R_{O_2} = a\ (\text{Chl}) + b$. The number of measurement pairs is given as n and the total depth range considered is Δz.

Station	a	b	r^2	n	Δz
10	0.1158	−0.0088	0.721	11	5–75
12	0.1242	0.0246	0.385	11	1–265
14	0.0977	0.0628	0.390	11	2–230
42	0.0616	0.0101	0.945	12	1–130
48	0.0408	−0.0149	0.933	10	1–145

$\text{min}^{-1}\ \text{m}^{-2}$, are presented in Table 9. Integrating respiration with depth by trapezoidal approximation has been used by many (Riley, 1951; Packard *et al.,* 1971; Eppley and Peterson, 1979). In our calculations that follow, the F_{trap} is always the highest estimate of carbon flux and the lowest variability around the mean value. The second way (Jenkins, 1982) integrates the R_{CO_2}-depth function ($R_z = R_t(z/z_t)^b$) as a definite integral from some upper depth (z_t), say 100 m, to infinity as the bottom depth. In the third way we use the depth of the bottom as the lower boundary for the definite integral. All integrations are presented in Table 9.

The indefinite integral of $R_z = R_t(z/z_t)^b$ with respect to depth (z) is:

$$F_c = \int R_t(z/z_t)^b\, dz = [R_t/((b+1)(z_t)^b)]\, z^{b+1} + C \tag{1}$$

where the first term represents the flux fueling the water-column respiration (F_{t-s}) and the constant, C, represents the flux fueling the respiration below the lower boundary (z_s), i.e., benthic respiration and carbon burial. Note that R_z, the respiration at any depth (z), and R_t, the respiration at the upper boundary depth (z_t), is R_{CO_2} and not R_{O_2}. Thus, the units are $\mu\text{mol C}\ \text{min}^{-1}\ \text{m}^{-3}$, while the total carbon flux (F_c) is in units of $\mu\text{mol C}\ \text{min}^{-1}\ \text{m}^{-2}$. To calculate the part of the flux (F_{t-s}) that is consumed in the water column between z_t and the bottom (z_s) we solve $R_z = R_t(z/z_t)^b$ as a definite integral between these two boundary conditions.

Table 6. R_{O_2} (Table 3) as a function of T_r in the form, $R_{O_2} = a \times T_r + b$. The number of measurement pairs is given as n and the total depth range considered is Δz.

Station	a	b	r^2	n	Δz
10	0.065	−0.4595	0.987	11	5–75
12	0.0859	−0.6067	0.782	9	1–100
14	0.0779	−0.5242	0.774	9	2–100
42	0.0267	−0.1404	0.931	12	1–130
48	0.0408	−0.2088	0.931	10	1–145

Table 7. T_r as a function of chlorophyll in the form, $T_r = a \times \text{Chl} + b$. The number of measurement pairs is given as n and the total depth range considered is Δz.

Station	a	b	r^2	n	Δz
10	1.6499	7.0227	0.659	12	5–75
12	1.6106	7.2154	0.750	10	1–100
14	1.4744	7.6344	0.602	10	2–100
42	2.0811	6.6202	0.828	12	1–130
48	0.9305	7.1693	0.927	12	1–145

$$F_{t-s} = \int_{Z_t}^{Z_s} R_t(z/z_t)^b \, dz = [R_t/((b+1)(z_t)^b)]\,[(z_s^{b+1}) - (z_t^{b+1})] \tag{2}$$

Here, z_t is 30, 50, or 100 m. Values of b and R_t for each station are given in Table 8. The carbon flux profiles from 30 m to the bottom are given in Figure 6. The averages of the five stations at 30, 50, and 90 m are shown in Table 9. F_{t-s} is always the lowest of the three integrations ($F_{\text{trap}} \geq F_{t-s} \leq F_\infty$), but its variability always falls between the others.

To calculate the carbon flux from z_t to infinity (F_∞), we find that in the limit as z_s goes to infinity, $[R_t/((b+1)(z_t)^b)]\,[(z_s^{b+1})]$ goes to zero. Thus

$$F_\infty = \int_{Z_t}^{\infty} R_t(z/z_t)^b \, dz = [R_t/((b+1)(z_t)^b)]\,[-z_t^{b+1}]. \tag{3}$$

Table 8. Equation parameters for the depth-normalized power function for respiratory CO_2 production, $R_{CO_2} = R_t(z/z_t)^b$, where R_{CO_2} is the modeled respiration in μmol C min^{-1} m^{-3} at any depth (z). Here, the constant, R_t represents R_{CO_2} (μmol C min^{-1} m^{-3}) at the upper boundary (z_t) of the depth interval considered. It is close to the measured value. The constant b is the curvature of the profile; b is always negative. The coefficient of determination (r^2) represents the goodness of fit when modeled R_{CO_2} is plotted linearly against R_{CO_2} calculated from R_{O_2} in Table 3. However, sometimes r^2 would approach 1 even as deeper values diverged widely from the measured ones or if R_{CO_2} was displaced from R_t by a constant. Consequently, the criterion for selecting R_t and b was not only the highest r^2, but also the closeness to 1 of the slope from the linear plot of modeled R_{CO_2} against R_{CO_2} calculated from R_{O_2} in Table 3.

Station	Depth (m)	Depth interval (m)	R_t	b	r^2	n
10	266	30–266	0.0199	−2.1730	0.956	6
12	275	25–275	0.1287	−2.6154	0.830	7
14	273	25–273	0.1668	−2.3917	0.963	7
42	147	30–147	0.0905	−1.8847	0.940	7
48	155	30–155	0.1713	−1.8537	0.753	8

Table 9. Carbon flux (F_c) from 30, 50, and 100 m in the GOM. (1) F_{trap}, is F_c from these depths (z_t) calculated by trapezoidal approximation. The bottom R value used in the F_{trap} calculation was the same as the minimum measured value at each station (Table 3). The depth of this value is z_s. (2) F_{t-s} is the integration of the normalized power function, $R_{CO_2} = R_t(z/z_t)^b$ (Table 8) between z_t and z_s. $F_{t-s} = [R_t/((1 + b)(z_t)^b)]\,[(z_s^{1+b}) - (z_t^{1+b})]$. (3) F_∞ is the integration of the same equation from Table 8 between the z_t and infinity (Jenkins, 1982). All three calculations represent the portion of F_c that is oxidized in the water column below z_t. All F_c values are given in μmol C min^{-1} m^{-2}. The grand mean and standard deviation (bold) in the lower right-hand corner of each of the three groups of data below has $n = 15$, not 3 or 5.

CARBON FLUX from 30 m.

Station	Bottom depth (m)	F_{trap}	F_{t-s}	F_∞	Mean	St. Dev. %
10	266	1.76	0.47	0.51	0.91	80
12	275	3.45	2.32	2.39	2.72	23
14	273	3.45	3.43	3.60	3.49	3
42	147	3.83	2.32	3.07	3.07	25
48	155	5.25	4.54	6.02	5.27	14
Mean		3.55	2.62	3.12	**3.09**	**50**
St. Deviation (%)		35	58	64		

CARBON FLUX from 50 m.

Station	Bottom depth (m)	F_{trap}	F_{t-s}	F_∞	Mean	St. Dev. %
10	266	1.52	0.26	0.30	0.69	103
12	275	2.09	0.98	1.05	1.37	45
14	273	2.12	1.60	1.77	1.83	14
42	147	2.22	1.20	1.95	1.79	30
48	155	3.04	2.41	3.89	3.11	24
Mean		2.20	1.29	1.79	**1.76**	**55**
St. Deviation (%)		25	61	75		

CARBON FLUX from 100 m.

Station	Bottom depth (m)	F_{trap}	F_{t-s}	F_∞	Mean	St. Dev. %
10	266	1.14	0.08	0.12	0.45	135
12	275	1.75	0.27	0.34	0.79	106
14	273	1.60	0.51	0.67	0.93	64
42	147	1.64	0.36	1.11	1.04	62
48	155	1.53	0.69	2.17	1.46	51
Mean		1.53	0.38	0.88	**0.93**	**73**
St. Deviation (%)		15	61	92		

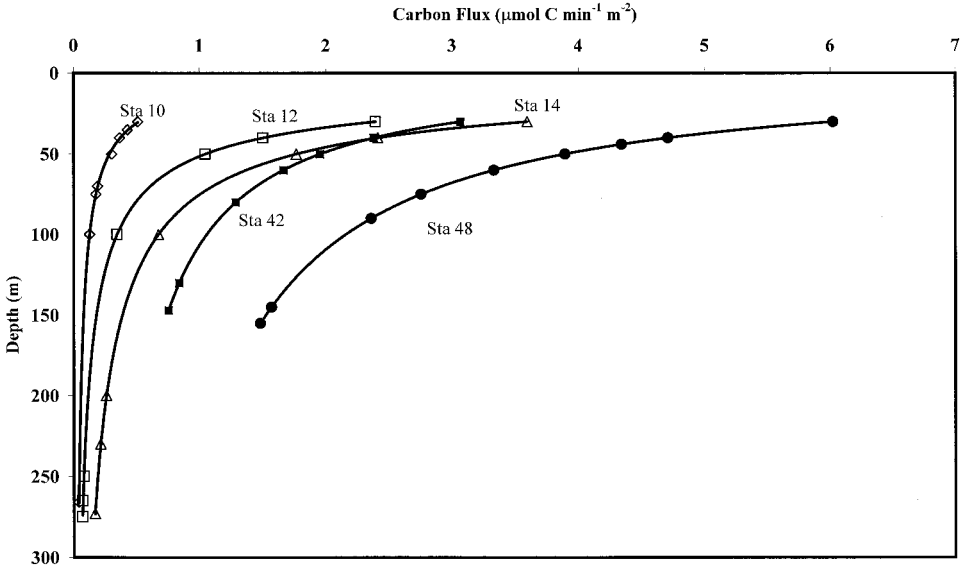

Figure 6. Carbon flux (F_∞) depth profiles for the Gulf of Maine, September 2002.

The results for this integration are also given in Table 9. F_∞ is always lower than F_{trap} and higher than F_{t-s} ($F_{\text{trap}} \geq F_\infty \geq F_{t-s}$), but its variability is always the highest. The average ($n = 15$) of all carbon fluxes calculations from 30 m (Table 9) is 3.09 ± 1.55 μmol C min^{-1} m^{-2}; for the 50 m it is 1.76 ± 0.96 μmol C min^{-1} m^{-2}; and for 100 m it is 0.93 ± 0.68 μmol C min^{-1} m^{-2}. The greatest analytical uncertainty in these calculations is the ±18% error associated with the Redfield ratio (Packard *et al.,* 1988). However, except for the 4 out of 15 calculations of standard deviation in Figure 6, the variability associated with the different stations and methods of integration is greater than ±18% (Table 9). This variability reflects the natural variability of F_c in the GOM region.

4. Discussion

a. Water column R_{O_2}

Seawater R_{O_2} calculated from ETS activity ranged from 30 to 680 pmol O_2 min^{-1} L^{-1} for the upper 30 m of the GOM (Table 3). Direct measurements in the upper 25 m in July 1980 in the GOM ranged from 1411 to 4124 pmol O_2 min^{-1} L^{-1} (Packard and Williams, 1981). ETS activities measured at the same time were similarly higher by a factor of 10. Respiration in the upper 30 m of the open Atlantic between Nova Scotia and Spain in September–October 1992 ranged from 350 to 760 pmol O_2 min^{-1} L^{-1} (Arístegui and Harrison, 2002). These measurements were calculated from ETS activities calibrated by direct measurements of R_{O_2} as they have been done here.

Table 10. Oceanic F_c calculations in μmol C min^{-1} m^{-2} by six different methods. Because the original F_c measurements were calculated for different time scales, the values have all been recalculated to facilitate comparison with our short time scale measurements. Original values have been used in the text.

Region	z (m)	F_c	Method	Scale	Reference
Atlantic, GOM	50	0.3–36	$^{234}Th/^{238}U$ disequilibria	days	(Benitez-Nelson *et al.,* 2000)
Atlantic, GOM	50	5–25	$^{234}Th/^{238}U$ disequilibria	days	(Charette *et al.,* 2001)
Atlantic, GOM	50	1.3–2.2	ETS	min	(This paper)
Atlantic, central, BATS	100	4.7–8.6	AOU/^{3}H-^{3}He dating	yr	(Jenkins, 1982)
Atlantic, central, BATS	100	7.9	AOU/^{3}H-^{3}He dating	yr	(Jenkins & Goldman, 1985)
Atlantic, central, BATS	100	4.8	AOU/^{3}H-^{3}He dating	yr	(Jenkins, 1998)
Atlantic, GOM	100	0.4–1.5	ETS	min	(This paper)
Pacific, northwest Vertex Stations	100	2.9	Sediment traps free floating	yr	(Martin *et al.,* 1987)
Pacific, central HOT Station	100	3.8	Mass balance model Emerson *et al.,* 1995	yr	(Emerson *et al.,* 1997)
Pacific, subarctic	100	6.1	Mass balance model	yr	(Andreev *et al.,* 2002)
All Oceans	100	0.7–33.3	$^{234}Th/^{238}U$ disequilibria	days	(Moran *et al.,* 2003)

b. Vertical fluxes of particulate organic carbon

F_c from the 30 m level ranged from 0.91 to 3.49 μmol C min^{-1} m^{-2} for Wilkinson Basin and from 3.07 to 5.27 μmol C min^{-1} m^{-2} on the southern Scotia shelf (Table 9). As expected F_c was lower at 50 m due to respiratory carbon consumption of the sinking particulate organic matter between the 30 m and the 50 m level. F_c at 50 m ranged from 0.69 to 1.83 μmol C min^{-1} m^{-2} for Wilkinson Basin and from 1.79 to 3.11 μmol C min^{-1} m^{-2} on the southern Scotia shelf (Table 9). F_c at 50 m by the $^{238}U/^{234}Th$ disequilibrium method in the GOM ranged from 0.3 to 36 (Benitez-Nelson *et al.,* 2000), and from 5–25 (Charette *et al.,* 2001) μmol C min^{-1} m^{-2} (Table 10). Our mean F_c from the 50 m level fell at the low end of this range (Table 9). Neither Benitez-Nelson *et al.* (2000) nor Charette *et al.* (2001), made F_c calculations from the 100 m level in the GOM, so we compared our calculations at this depth with those made in the Sargasso Sea and other parts of the world ocean (Table 10).

For the 100 m level, our mean F_c ranged from 0.45 to 1.45 μmol C min^{-1} m^{-2} (Table 9). In the northern Sargasso Sea at this depth F_c ranged from 4.7 to 8.6 μmol C min^{-1} m^{-2} by the ^{3}He-^{3}H method (Jenkins, 1982). In the northern Pacific Ocean it ranged from 2.9 to 6.1 μmol C min^{-1} m^{-2} according to methods based on mass balance models and sediment

traps (Table 10). An overall oceanic range for 100 m is 1–33 μmol C m^{-2} min^{-1} according to different investigations based on the $^{238}U/^{234}Th$ method (Moran *et al.,* 2003). Note that the time-scale inherent in each method is different. F_c from ETS activities and ^{238}U to ^{234}Th decay are based on minute-scale changes, F_c from ^{3}He-^{3}H method are based on annual-scale changes, and F_c from sediment traps are based on day-to-month scale changes. Thus, to compare the short-time-scale methods with the long-time-scale ones, time-series data for the short-time-scale methods is needed. Nevertheless, our mean F_c of 0.45 to 1.45 μmol C min^{-1} m^{-2}, surprisingly, fell at the low end of oceanic measurements. One would expect higher values in coastal waters than oceanic ones, but considering the time-scale differences of the measurements and the punctuated nature of events in biogeochemistry, this difference is not remarkable. Nevertheless, an ETS and R_{O_2} time-series investigation at any station, coastal or oceanic, where the annual variability of F_c has been well studied, would help to explain it.

c. Uncertainty in R_{O_2} and F_c calculations

A recent discussion of uncertainty and variability in F_c calculations and measurements reveals variability that ranges from factors of 3 to 10 for sediment-trap measurements and from 2 to 10 for the $^{238}U/^{234}Th$ disequilibrium method (Moran *et al.,* 2003). What uncertainty and variability is inherent in the ETS method? Variability in assessing oceanographic processes is normal. Just as there is variability in the region-to-region chlorophyll algorithm for satellite imagery, variability in the paleotemperature estimates from fossilized alkenones in marine sediments, and variability in all of the conversion factors for the popular ecological indices for microbial metabolism, there will be variability in the ETS assessment of R_{O_2}. Some of this variability with the ETS method has been discussed before. Calculations based on different ETS methodologies had uncertainties ranging from ±24% to ±33% (Packard *et al.,* 1988). Working with the same methodology used here, Arístegui and Montero (1995) found uncertainties ranging from ±22% to ±72%, but their mean uncertainty was ±34%. Here, the analytical error for duplicate ETS analyses was ±7.8% (Table 4). However, the overall uncertainty in a prediction of R_{O_2} from ETS is dictated by the uncertainty of the *R*/ETS ratio ($C_{R/ETS}$) in Figure 2, namely ±12%. The ratio of 0.26 may change seasonally and annually, but here we assume it does not change. The error involved in this assumption can only be resolved by time-series studies, preferably in the GOM. The ratio, $C_{R/ETS}$, may also change as the composition of the plankton community changes with depth. However, our research with marine bacteria in culture suggests that it may not change so much. $C_{R/ETS}$ in growing *Pseudomonas nautica,* a marine bacterium, is 0.24 ± 0.01 (Packard *et al.,* 1996), close to 0.26, the value we have used here. Nevertheless, this uncertainty needs to be resolved by both field and laboratory studies. Finally, calculating carbon flux from R_{O_2} requires a Redfield ratio that has an uncertainty of ±18%. So for all the known uncertainties this one will dominate the calculations here (Table 9 and Fig. 6).

d. R_{O_2} models for the deep ocean

We used a power function to describe the rapidly decreasing R_{O_2} in the ocean water column, however for discussion we refer to it as an exponential decrease. Whether it is really a power function, a logarithmic function, or an exponential function is still a question whose resolution requires more detailed resolution of $R_{O_2} = f(z)$. Until that time it would be profitable to consider what drives respiration in the oceanic water column. Microorganisms are ubiquitous in the ocean and will respond by growth or migration to any source of nourishment. Certainly the overwhelming source is POC, produced in the euphotic zone, that sinks as fecal pellets, moribund cells, debris from sloppy feeding, eggs, and exuviae. However, there are other sources to consider. (1) Resuspension of POC and injection of DOC near the ocean floor (nephaloid layer) via bioturbation and bottom currents. (2) POC and DOC injection from the deep sea vent systems and their biological communities. (3) Exuviae, excretion, and bodies of vertically migrating zooplankton and nekton. All of these mechanisms are sources of nourishing organic matter for the deep sea. On two of our stations (12 and 42) the near bottom sample showed elevated R_{O_2} suggesting resuspension of POC and injection of DOC near the ocean floor via benthic bioturbation and bottom currents. Were we able to sample at meter intervals above the bottom we might have seen R_{O_2} increasing exponentially towards the bottom. Were this the general case, then $R_{O_2} = f(z)$ might require a second term to describe this benthic source. As a heuristic exercise, we added a power function, which increased R_{O_2} with depth, to the exponential depth decreasing functions for stations 12 and 42. The composite equations showed an increase in R near the bottom with a high coefficient of determination (r^2) but with only a point for each profile we decided not to pursue the topic further. Still, the exercise hinted of a more complex function, $R_{O_2} = f(z)$, in the benthic boundary layer.

In addition to different sources of organic nourishment in the deep sea there are different mechanisms that influence the distribution of the organic matter. Gravity leads to a steady rain of material from the euphotic zone into the depths. However, interleaving water masses with their different levels of entrained POC and DOC can lead to different background levels on which the rain of POC is superimposed. Also in zones of deep-water formation the exponential decrease of the raining POC could be completely obscured by entrained organic matter. Thus $R_{O_2} = f(z)$ should look different in these regions. Furthermore, below the pycnocline and below the depth where much of the nucleic acids and proteins have been remineralized to NO_3^-, NH_4^+, and PO_4^{-3}, the lipid enriched POC should settle at lower rates. The effect of this would be to give the deepwater organisms relatively more time to oxidize the sinking POC. This might explain why the depth decrease of R_{O_2} (dR_{O_2}/dz) in the deep-sea decreases to nearly a linear function (Packard *et al.,* 1971).

Concerning the impact of food sources and food distribution mechanisms on oceanic R_{O_2} and F_c, we conclude the following from this discussion above. A better understanding of the coupling between oceanographic and metabolic processes would follow if water-column studies of R_{O_2} were focused on: (1) benthic boundary layers; (2) the vicinity of

deep sea vents; (3) interleaving water masses (e.g., Mediterranean water in the Atlantic); (4) and sinking water masses (e.g., Labrador Sea).

5. Conclusion

Water column R_{O_2} calculated from ETS activity in filtered particulate matter ranged from 30 to 680 pmol O_2 min^{-1} L^{-1} for the upper 30 m of the Gulf of Maine in September 2002. The vertical profiles below the subsurface maximum are best described by a depth-normalized power function ($R_z = R_t(z/z_t)^b$). Carbon fluxes from 30, 50, 100 m were 3.09 ± 1.55, 1.76 ± 0.96, and 0.93 ± 0.86 μmol C min^{-1} m^{-2} (n = 15), respectively (Table 9). Each of these values is based on five vertical profiles of respiration integrated three different ways. These results fall at the low end of the published oceanic and GOM carbon fluxes, but demonstrate that the ETS method provides an additional way to assess carbon flux in the ocean.

Acknowledgments. We thank Miguel Alcaraz, Elisa Berdalet, Dolors Blasco, Marta Estrada, Kjell Gundersen, and Lynne Butler without whose aid, advice, and good will, we would not have accomplished this research. We acknowledge the Institut Ciències del Mar, CICYT project MAR98-0932, BIOHAB project EVK3-1999-00072, and ONR contract N00014-02-1-4094 for financial support.

REFERENCES

Andreev, A., M. Kusakabe, M. Honda, A. Murata and C. Saito. 2002. Vertical fluxes of nutrients and carbon through the halocline in the western Subarctic Gyre calculated by mass balance. Deep-Sea Res. II, *49,* 5577–5593.

Arístegui, J., S. Agusti and C. M. Duarte. 2003. Respiration in the dark ocean. Geophys. Res. Lett., *30,* 1041.

Arístegui, J. and W. G. Harrison. 2002. Decoupling of primary production and community respiration in the ocean: implications for regional carbon studies. Aquatic Microb. Ecol., *29,* 199–209.

Arístegui, J. and M. F. Montero. 1995. The relationship between community respiration and ETS activity in the ocean. J. Plankton Res., *17,* 1563–1571.

Benitez-Nelson, C., K. O. Buesseler and G. Grossin. 2000. Upper ocean carbon export, horizontal transport, and vertical eddy diffusivity in the southwestern Gulf of Maine. Cont. Shelf Res., *20,* 707–736.

Charette, M. A., S. B. Moran, S. M. Pike and J. N. Smith. 2001. Investigating the carbon cycle in the Gulf of Maine using the natural tracer thorium-234. J. Geophys. Res., *109,* 11,553–11,579.

Christensen, J. P., T. T. Packard, F. Q. Dortch, H. J. Minas, J. C. Gascard, C. Richez and P. C. Garfield. 1989. Carbon oxidation in the deep Mediterranean Sea: evidence for dissolved organic carbon source. Global Biogeochem. Cycles, *3,* 315–335.

Del Giorgio, P. A. 1992. The relationship between ETS (electron transport system) activity and oxygen consumption in lake plankton: a cross-system calibration. J. Plankton Res., *14,* 1723–1741.

Emerson, S., P. Quay, D. Karl, C. Winn, L. Tupas and M. Landry. 1997. Experimental determination of the organic carbon flux from open-ocean surface waters. Nature, *389,* 951–954.

Eppley, R. W. and B. J. Peterson. 1979. Particulate organic matter flux and planktonic new production in the deep ocean. Nature, *282,* 677–680.

Fruton, J. S. and S. Simmonds. 1961. General Biochemistry, John Wiley & Sons Inc, NY 1077 pp.

Garfield, P. C., T. T. Packard, G. E. Friederich and L. A. Codispoti. 1983. A subsurface particle maximum layer and enhanced microbial activity in the secondary nitrate maximum of the northeastern tropical Pacific. J. Mar. Res., *41,* 747–768.

Hopkins, T. S. and N. Garfield. 1979. Gulf of Maine intermediate water. J. Mar. Res., *37,* 103–139.

Jenkins, W. J. 1982. Oxygen utilization rates in North Atlantic subtropical gyre and primary production in oligotrophic systems. Nature, *300,* 246–248.

—— 1998. Studying subtropical thermocline ventilation and circulation using tritium and ^{3}He. J. Geophys. Res., *103 (C8),* 15,817–15,831.

Jenkins, W. J. and J. C. Goldman. 1985. Seasonal oxygen cycling and primary production in the Sargasso Sea. J. Mar. Res., *43,* 465–491.

Kenner, R. A. and S. I. Ahmed. 1975. Correlation between oxygen utilization and electron transport activity in marine phytoplankton. Mar. Biol., *33,* 129–133.

Madigan, M. T., J. M. Martinko and J. Parker. 2000. Brock Biology of Microorganisms. Prentice Hall, 991 pp.

Martin, J. H., G. A. Knauer, D. M. Karl and W. W. Broenkow. 1987. VERTEX: carbon cycling in the northeast Pacific. Deep-Sea Res., *34,* 267–285.

Moran, S. B., S. E. Weinstein, H. N. Edmonds, J. N. Smith, R. B. Kelly, M. E. Q. Pilson and W. G. Harrison. 2003. Does ^{234}Th/^{238}U disequilibrium provide an accurate record of the export flux of particulate organic carbon from the upper ocean? Limnol. Oceanogr., *48,* 1018–1029.

Munk, W. H. 1966. Abyssal Recipes, Deep-Sea Res., *13,* 707–730.

Nelson, D. L. and M. M. Cox. 2000. Lehninger Principles of Biochemistry, Worth Publishers, NY, 1152 pp.

Packard, T. T., E. Berdalet, D. Blasco, S. Roy, L. St. Amand, B. Lagace, K. Lee and J. Gagne. 1996. Oxygen consumption in the marine bacterium, *Pseudomonas nautica* predicted from ETS activity and bisubstrate enzyme kinetics. J. Plankton. Res., *18,* 1819–1835.

Packard, T. T., W. Chen, D. Blasco, C. Savenkoff, A. F. Vezina, R. Tian, L. St. Amand, S. O. Roy, C. Lovejoy, B. Klein, J. C. Therriault, L. Legendre and R. G. Ingram. 2000. Dissolved organic carbon in the Gulf of St. Lawrence. Deep-Sea Res. II, *47(3–4),* 435–459.

Packard, T. T., M. Denis, M. Rodier and P. Garfield. 1988. Deep-ocean metabolic CO_2 production: calculations from ETS activity. Deep-Sea Res., *35,* 371–382.

Packard, T. T., A. H. Devol and F. D. King. 1975. The effect of temperature on the respiratory electron transport system in marine plankton. Deep-Sea Res., *22,* 237–249.

Packard, T. T., P. C. Garfield and R. Martinez. 1983. Respiration and respiratory enzyme activity in aerobic and anaerobic cultures in the marine denitrifying bacterium *Pseudomonas perfectomarinus.* Deep-Sea Res., *30,* 227–243.

Packard, T. T., D. Harmon and J. Boucher. 1974. Respiratory electron transport activity in plankton from upwelled waters. Tethys, *6 (1–2),* 213–222.

Packard, T. T., M. L. Healy and F. A. Richards. 1971. Vertical distribution of the activity of the respiratory electron transport system in marine plankton. Limnol. Oceanogr., *16,* 60–70.

Packard, T. T. and P. L. B. Williams. 1981. Rates of respiratory oxygen consumption and electron transport in surface seawater from the northwest Atlantic Ocean. Oceanologica Acta, *4,* 351–358.

Prahl, F. G., C. H. Pilskaln and M. A. Sparrow. 2001. Seasonal record for alkenones in sedimentary particles from the Gulf of Maine. Deep-Sea Res. I, *48,* 515–528.

Redfield, A. C. 1942. The processes determining the concentration of oxygen, phosphate and other organic derivatives within the depths of the Atlantic Ocean *in* Papers on Physical Oceanography and Meteorology, Massachusetts Institute of Technology and the Woods Hole Oceanographic Institution, Cambridge and Woods Hole, Massachusetts, 1–22.

Riley, G. A. 1951. Oxygen, phosphate, and nitrate in the Atlantic Ocean. Bull. Bingham Oceanogr. Collection, *13,* 1–169.

Savenkoff, C., T. T. Packard, M. Rodier, M. Gerino, D. Levevre and M. Denis. 1995. Relative contribution of dehydrogenases to overall respiratory ETS activity in some marine organisms. J. Plankton Res., *17,* 1593–1604.

Suess, E. 1980. Particulate organic carbon flux in the oceans: Surface productivity and oxygen utilization. Nature, *288,* 260–263.

Takahashi, T., W. S. Broecker and S. Langer. 1985. Redfield ratio based on chemical data from isopycnal surfaces. J. Geophys. Res., *90 (C4),* 6907–6924.

Tortell, P. D., M. T. Maldonado and N. M. Price. 1996. The role of heterotrophic bacteria in iron-limited ocean ecosystems. Nature, *383,* 330–332.

Received: *6 August, 2003;* revised: *11 January, 2004.*